Title: A novel surfactant protein is associated with extrapulmonary respiration in lungless salamanders

Short title: Novel surfactant protein in salamanders

Authors: Zachary R. Lewis,[1,2*] Jorge A. Dorantes,[1,3] James Hanken[1]

Institutions:

[1] Department of Organismic and Evolutionary Biology and Museum of Comparative Zoology, Harvard University, Cambridge, MA, USA, 02138

[2] Present address: Department of Ecology and Evolutionary Biology, Yale University, New Haven, CT, USA, 06511

[3] Present address: Universidad Autónoma de Guadalajara, Facultad de Medicina, Guadalajara, Jalisco, C.P. 44100, México

[*] To whom correspondence should be addressed

E-mail: zrlewis@gmail.com

Address: 165 Prospect St, New Haven, CT, 06511

Telephone: 1-206-920-3567

Keywords: Salamander, respiration, gene duplication, molecular evolution, surfactant, plethodontid

Abstract: Numerous physiological and morphological adaptations were achieved during the transition to lungless respiration following evolutionary lung loss in plethodontid salamanders, including those that enable efficient gas exchange across extrapulmonary tissue. However, the molecular basis of these adaptations is unknown. Here we show that lungless salamanders express in the skin and buccal cavity—the principal sites of respiratory gas exchange in these species—a novel paralog of the gene Surfactant-Associated Protein C (SFTPC), which is a critical component of pulmonary surfactant expressed exclusively in the lung in other vertebrates. The paralogous gene appears to be found only in salamanders, but, similar to SFTPC, in lunged salamanders it is expressed only in the lung. This heterotopic gene expression, combined with predictions from structural modeling and respiratory tissue ultrastructure, suggest that lungless salamanders produce pulmonary surfactant-like secretions outside the lungs and that the novel paralog of SFTPC might facilitate extrapulmonary respiration in the absence of lungs. Heterotopic expression of the SFTPC paralog may have contributed to the remarkable evolutionary radiation of lungless salamanders, which account for more than two thirds of urodele species alive today.

Introduction: Most amphibians must confront the challenges of respiring both in water and on land. To do so, they utilize numerous gas exchange surfaces including the lungs, gills, integument and buccopharyngeal mucosa, which are employed to varying extents depending on species and life-history stage. In adult salamanders, for example, the integument may be responsible for 50% or more of oxygen uptake [1,2]. Lability in sites of gas exchange is especially critical for metamorphosing species, which face different respiratory demands in air and water. Little is known, however, about the molecular mechanisms that enable the ontogenetic and evolutionary transitions from aquatic to aerial respiration. The mechanism of aerial respiration is even more enigmatic in lungless species, which rely entirely on extrapulmonary sites of respiration [1–3]. The family Plethodontidae includes more than two thirds of all living salamander species; most are fully terrestrial, and all adults lack lungs. Respiration takes place solely across the integument and buccopharyngeal mucosa, and also across the gills in aquatic larval forms, when present. Lunglessness is not unique to plethodontids—it has evolved several times in other amphibians, including salamanders, frogs and caecilians [4]—but its adaptive significance is unresolved [5,6].

How lungless salamanders are able to satisfy metabolic demands for oxygen is a topic of considerable interest. In theory, lunglessness limits thermal tolerance and maximum body size, yet lungless salamanders paradoxically occupy diverse thermal environments and attain relatively large body sizes. Plethodontids

63 possess highly vascularized skin and buccopharyngeal mucosa, which may
64 compensate for the loss of pulmonary respiration [1,7–9]. The buccopharyngeal
65 membranes, in particular, may function as an adaptive respiratory surface that
66 facilitates gas exchange, as evidenced by increased oscillation of the floor of the
67 buccal cavity under hypoxia, high temperature, or activity, which presumably
68 serves to draw more air into the mouth [1,7,10]. Selection for efficient
69 extrapulmonary respiration may have played a major role in the adaptive
70 radiation of terrestrial plethodontids [1]. Indeed, the evolution of highly efficient
71 cutaneous and buccopharyngeal respiration is believed to have freed
72 plethodontids from the ontogenetic and functional constraints associated with the
73 use of a buccal pump for pulmonary ventilation, thereby enabling them to occupy
74 diverse habitats and evolve ballistic tongue projection [2,11,12].
75
76 To identify the molecular adaptations that might facilitate lungless respiration, we
77 investigated the expression of a crucial pulmonary surfactant-associated protein
78 in plethodontid salamanders. Proper lung function requires pulmonary surfactant,
79 a complex and evolutionarily variable mix of molecules that facilitate mucous
80 spreading and lung compliance and improve oxygen diffusion [13–15].
81 Surfactant-associated protein C (SFTPC) is a hydrophobic protein found in
82 pulmonary surfactant that localizes to the lung's air-liquid interface. It reduces
83 surface tension by aiding the adsorption and distribution of lipids within
84 pulmonary surfactant and specifically enhances oxygen diffusion [14,16,17].
85 SFTPC also regulates production and turnover of phosphatidylcholine, a major

86 component of pulmonary surfactant, and it limits the thickness of the hypophase,
87 the liquid layer that lines the lung's inner surface [18–20]. Mucous layer thickness
88 greatly impacts gas exchange between the environment and the blood supply
89 [21]. Additionally, oxygen uptake is enhanced by the presence of surfactant in the
90 hypophase, likely due to convective effects that facilitate mixing of oxygen and
91 mucous or increased rate of oxygen trafficking [15,22]. The expression of SFTPC
92 is highly conserved among tetrapods: all species evaluated previously express
93 SFTPC exclusively in the lungs [23–25] (and Supplementary Text).
94
95 **Results and Discussion:** Despite lacking lungs as adults, plethodontid
96 salamanders express SFTPC (Fig. S1). Due to the consistent restriction of
97 SFTPC expression to the lungs and to SFTPC's conserved role across tetrapods,
98 we compared SFTPC expression between lungless and lunged salamanders.
99 Surprisingly, several species of salamanders express two transcripts with high
100 sequence identity to annotated SFTPC sequences (Fig. S1a, b). Both transcripts
101 exclusively match SFTPC within the NCBI nucleotide collection database, but
102 one possesses higher sequence similarity to amniote and frog SFTPC. We
103 denote the transcript with lower similarity SFTPC-like. We did not find SFTPC-
104 like within vertebrate genomes or transcriptomes outside of salamanders.
105 Phylogenetic analyses support the hypothesis that SFTPC-like represents a
106 previously undescribed salamander-specific paralog of the highly conserved
107 lung-specific gene, SFTPC (Figs. S1, S3; Supplementary Text). SFTPC-like may

maintain or partially maintain the characteristic hydrophobic alpha-helical configuration of the SFTPC mature peptide [16] (Fig. S1c).

Numerous studies of tetrapods localize SFTPC exclusively to the lungs [23–25]. SFTPC and SFTPC-like in the lunged salamander *Ambystoma mexicanum* match this highly conserved pattern (Fig. 1). As visualized by *in situ* hybridization, SFTPC and SFTPC-like staining is only observed in the extremely squamous alveolar epithelial cells lining the lungs and trachea (Figs. 1, S5, S6). SFTPC-like expression, however, is lower than SFTPC and the genes are expressed at different times: SFTPC-like is low or non-existent before hatching, whereas SFTPC is expressed beginning in embryos immediately following the formation of the laryngotracheal groove, a ventral outpocketing of the foregut that precedes lung outgrowth (Fig. 1a, b), and continuing into adulthood (Fig. 1d).

In contrast, SFTPC-like is expressed dynamically in lungless salamanders. In embryos and early larvae of *Desmognathus fuscus*, a metamorphosing species, SFTPC-like is expressed throughout much of the integument, with reduced staining on the dorsal (internal) surface of the operculum (gill covering) and in the limbs (Fig. 2a–h). Expression begins to diminish in the integument immediately before metamorphosis, but at the same time it expands to the buccopharyngeal mucosa (oral epithelium) (Fig. 2i–l). Integumentary expression at this stage is patchy: remaining SFTPC-like-positive cells are displaced towards the apical surface and display an irregular morphology (Fig. 2i, k). Cessation of

131 integumentary expression of SFTPC-like coincides with several metamorphic
132 transitions, but especially molting [26], when the integument is profoundly
133 remodeled from a simple stratified epithelium to a thickened pseudostratified
134 tissue rich in acinous glands (Fig. S4, Fig. 2i, k).
135
136 Immediately following metamorphosis, expression is absent from the integument
137 and restricted to the buccopharyngeal mucosa (Fig. 2m–r). In adults, SFTPC-like
138 is expressed in the buccal cavity and adjacent pharynx (Fig. 2m–r): it is confined
139 to oral mucosa, with a strict boundary at the marginal teeth. SFTPC-like is not
140 expressed along the vomerine bones (near the internal nares) or in the dorsal
141 midline of the tongue, although it is strongly expressed along the tongue margin
142 (Fig. 2m, o). Additional data from immunohistochemistry and mass spectroscopy
143 are needed to determine if SFTPC-like transcripts are translated and whether this
144 protein is then processed and secreted in a similar fashion to SFTPC in the lung.
145
146 Unlike SFTPC-like, SFTPC is expressed at an extremely low level in embryos of
147 lungless species, which develop a transient lung rudiment [27]. The SFTPC
148 transcript detected from transcriptome sequencing of the lung rudiment of
149 *Plethodon cinereus* (Supplemental Data File 1) could not be cloned from either *P.*
150 *cinereus* or *D. fuscus*, nor was it found in adult plethodontid transcriptomes. This
151 suggests that SFTPC expression is inhibited by lung loss in lungless species,
152 with the exception of SFTPC expression at certain embryonic stages in the
153 presumptive lung region.

154

155 The larval integument of *Desmognathus fuscus* displays pronounced secretory
156 activity (Fig. 3a–d). The outer layer—the stratum corneum—is a protective layer
157 composed of anuclear keratinized cells. It displays an extremely high level of
158 secretory activity evidenced by the near universal distribution of bilamellar
159 secretory vesicles along its superficial surface (Fig. 3a, “SV”). Just basal to the
160 stratum corneum is a layer of secretory cells, which are heavily vacuolated at
161 their apical extent. The stratum corneum and the layer of secretory cells are not
162 separated by a cell membrane, but a dark and consistent division appears
163 between them (Fig. 3b). Bilamellar secretory vesicles virtually identical to those
164 observed on the stratum corneum of *D. fuscus* are secreted from alveolar
165 epithelial cells in the lung of *Ambystoma mexicanum* but are not present in its
166 integument (Fig. 3e, g, h; Fig. S6, “SV”).

167

168 Pulmonary surfactant is trafficked in lamellar bodies in alveolar epithelial cells.
169 These lamellar bodies are distinct from other ultrastructural lamellar elements in
170 that they are large in diameter and spherical in shape [28–30]. Furthermore,
171 these lamellar bodies are distinct from the bilamellar structures identified on the
172 surface of the integument, in that they have many lamellae. The larval
173 integument of *D. fuscus* contains large (0.5–0.75 μm diameter), spherical
174 lamellar bodies (Fig. 3c, d, “LB”) that closely resemble those found in alveolar
175 epithelial cells, which otherwise are known only from the lungs of other
176 tetrapods.. Secretory activity and the presence of these distinctive lamellar

bodies strongly suggest that *D. fuscus* produces surfactant in extrapulmonary sites of gas exchange, which correspond to sites of SFTPC-like expression.

Despite the lung- and trachea-specific expression of SFTPC and SFTPC-like in *A. mexicanum* revealed by *in situ* hybridization and the numerous reports of lung-specific expression of SFTPC in mammals (Supplementary text), recently published transcriptomes of *A. mexicanum* purport to map low numbers of SFTPC and SFTPC-like reads to several tissues, including blood vessels, bone, heart, regenerating limbs, and mixed stages of whole embryos [31]. Therefore, SFTPC and SFTPC-like may not be entirely lung-specific transcripts in lunged salamanders. Additional studies are needed, however, to evaluate the alternative interpretation that contamination, mapping or assembly issues might have yielded spuriously mapped reads.

Passive diffusion across a tissue layer, as occurs during cutaneous respiration, is a function of several variables. These include the size (area) of the surface over which gas exchange occurs and the thickness of the barrier between the underlying blood supply and the environment [3]. Barrier thickness depends mainly on the distance between the environment and the blood supply, but also on the thickness of the mucous layer between the environment and respiratory tissue. Diffusivity of mucus is about 30% lower than water [21]. Reduction of surface tension by pulmonary surfactant helps maintain a thin layer of airway surface liquid [20] and increases convection within the mucous, which together

result in increased oxygen uptake [22]. SFTPC indirectly influences mucous layer thickness in the lung by regulating the production of phosphatidylcholine [18]. Pulmonary surfactant aids oxygen transport across the air-liquid interface, and hydrophobic surfactant proteins increase the rate of oxygen diffusion twofold over surfactant lipid alone [15,17]. SFTPC-like may facilitate respiration through a reduction of effective barrier thickness or an increase in diffusivity of the mucus layer. Pulmonary surfactant also plays non-respiratory roles, including facilitation of mucus spreading, innate immune defense, anti-edema agent, hydrostatic gas exchange, and preventing adhesion of lung surfaces when the lungs deflate [13,32,33]. It is possible that extrapulmonary surfactant produced in *Desmognathus fuscus* is performing one or more of these functions instead of, or in addition to, facilitating gas exchange.

Spatial and temporal expression of SFTPC-like and the ultrastructure of the associated integument suggest that, following SFTPC-gene duplication, SFTPC-like became neofunctionalized for extrapulmonary respiration in lungless salamanders. Sequence and structural conservation of SFTPC-like and SFTPC suggests that the two proteins function similarly (Fig. S1). However, to confirm neofunctionalization requires a more detailed functional characterization of SFTPC-like. This may include determining with increased phylogenetic and technical precision how expression of SFTPC-like has evolved in salamanders, proteomic characterization of skin and buccopharyngeal secretions, and

222 assessment of whether SFTPC-like displays surface activity or aids gas
223 exchange.
224
225 In metamorphosing species such as *Desmognathus fuscus*, respiratory and fluid-
226 retention demands shift dramatically upon the transition from aquatic to terrestrial
227 habitats [1]. Cutaneous water loss becomes a critical liability, but reduced skin
228 permeability hinders cutaneous gas exchange. To counter this limitation,
229 terrestrial plethodontids show increased reliance on buccopharyngeal respiration
230 [1]. Ontogenetic shift of SFTPC-like from the skin to the buccopharyngeal cavity
231 during metamorphosis (Fig. 2) correlates with the transition from aquatic to aerial
232 respiration; SFTPC-like is expressed at the preferential sites of gas exchange at
233 each life-history stage [1]. However, it is also possible that instead of playing a
234 direct role in facilitating gas exchange, extrapulmonary surfactant balances fluid
235 retention and respiratory demands by aiding fluid uptake from the mucus. Such a
236 role would be consistent with the proposed anti-edema properties of surfactant
237 within the lungs [13].
238
239 Gene duplication is increasingly recognized as a driving force of evolutionary
240 innovation [34]. While gene duplication does not always lead to functional
241 divergence [35,36], regulatory changes in duplicated genes, such as altered
242 expression sites, may enable the evolution of novel traits in individual lineages.
243 Many studies of the evolutionary phenomenon of adaptive radiation have
244 emphasized morphological traits whose appearance in particular lineages

245 promote phylogenetic and ecological diversification [37]. We propose that such
246 morphological traits, or key adaptations, work in concert with novel and
247 functionally significant molecular features to enhance evolutionary success, and
248 that such instances of concerted evolution are more widespread than is currently
249 recognized.
250
251 In plethodontid salamanders, it is possible that the combination of morphological
252 adaptations [7,9,38] and novel deployment of a critical surfactant protein enables
253 efficient extrapulmonary respiration via the buccopharynx and integument.
254 Conserved expression of SFTPC-like in lunged salamanders relative to SFTPC
255 may be due to dosage-sharing between SFTPC and SFTPC-like, which
256 constrains tolerable mutations in SFTPC-like gene regulation [35]. Indeed, lung
257 loss may have resulted in relaxed stabilizing selection for SFTPC-like gene
258 regulation, thereby enabling the evolution of novel expression patterns. Greater
259 understanding of the evolution and function of SFTPC-like in additional
260 salamander species will yield a more complete picture of the evolution and
261 consequences of lung loss, while functional studies of SFTPC-like promise to
262 reveal whether this novel pulmonary surfactant protein plays similar roles to
263 SFTPC or has potential therapeutic applications. Given the convergent evolution
264 of lung loss in several amphibian lineages, it will be interesting to investigate the
265 molecular physiology of other lungless taxa. Neofunctionalization of SFTPC-like
266 may represent an additional mechanism by which plethodontid salamanders
267 have become one of the most speciose and geographically widespread clades of

268 vertebrates on earth, despite the theoretical limitations on thermal tolerance and
269 body size imposed by lunglessness.
270

271 **Materials and Methods:**

272 **Animal husbandry**

273 All animal protocols were reviewed and approved by Harvard's Institutional
274 Animal Care and use Committee (protocol 99-09). *Desmognathus fuscus*
275 (Northern dusky salamander) embryos were field-collected from the following two
276 localities under Massachusetts Department of Fish and Wildlife collection permits
277 080.11SCRA (2012), 027.13SCRA (2013), 083.14SCRA (2014), and
278 022.15SCRA (2015) and appropriate local permits: Ashfield, Mass. (42.483111, -
279 72.761263) and Mass Audubon Wachusett Meadows Preserve (42.450922, -
280 71.913009). Adults were collected from Willard Brook State Forest (42.671606, -
281 71.776156). *Plethodon cinereus* (Eastern red-backed salamander) embryos were
282 field collected from Willard Brook State Forest (42.671606, -71.776156).
283 *Desmognathus fuscus* embryos were maintained at 15°C in 0.1x Marc's Modified
284 Ringer solution (MMR; 0.01 M NaCl, 0.2 mM KCl, 0.1 mM $MgSO_4$, 0.2 mM $CaCl_2$,
285 0.5 mM HEPES pH 7.4). Following hatching, larvae were fed *Artemia* spp. and
286 maintained at 17–20°C until they metamorphosed at approximately seven
287 months post-hatching. Older larvae were hand-fed blood worms. Embryos and
288 larvae were sampled at intermediate stages from embryogenesis until 3–5 days
289 post-metamorphosis and fixed overnight in MEMFA (0.1 M MOPS pH 7.4, 2 mM
290 EGTA, 1 mM $MgSO_4$, 3.7% formaldehyde) at 4°C, then dehydrated and stored at

291 -20°C in 100% methanol. Adults were fixed in a similar manner immediately upon
292 collection.

293 *Ambystoma mexicanum* (Mexican axolotl) embryos were obtained from the
294 *Ambystoma* Genetic Stock Center, University of Kentucky, and maintained in
295 20% Holtfreter solution at 17°C. Larvae were raised similarly to larval
296 *Desmognathus fuscus*. Fixation was performed as described above.

297 *Ambystoma mexicanum* were staged according to [39,40]. *Desmognathus fuscus*
298 embryos were staged using a staging table derived for *Plethodon cinereus*, as
299 their developmental timing and morphology are grossly similar [41].

300 **PCR**

301 Embryonic cDNA from *Desmognathus fuscus*, *Plethodon cinereus*, and
302 *Ambystoma mexicanum* was used to clone the gene SFTPC-like. RNA was
303 isolated from homogenates of whole animals at a variety of embryonic stages
304 using TRIzol Reagent (Invitrogen/Thermo Fisher Scientific, Grand Island, N.Y.)
305 and reverse-transcribed to cDNA using iScript reverse transcriptase (BioRad,
306 Hercules, Calif.). The gene SFTPC was cloned from *A. mexicanum* and repeated
307 attempts were made to clone SFTPC from plethodontids. Degenerate and non-
308 degenerate PCR primers were used (Table S1).

309 Primers were designed based on alignment of SFTPC sequences from
310 *Desmognathus fuscus*, *Xenopus laevis*, *X. tropicalis*, *Anolis carolinensis*,
311 *Neovison vison*, *Bos taurus*, *Monodelphis domesticus*, and *Homo sapiens*. All

sequences but one were obtained from GenBank; the *D. fuscus* sequence was kindly provided by Dr. David Weisrock.

Transcriptome assembly

Transcriptomes for *Plethodon cinereus* and *Ambystoma mexicanum* were prepared from microdissected tissue from pharyngeal endoderm and mesoderm of embryos and from the lung of a juvenile *A. mexicanum*. Total RNA was utilized for library preparation by using the IntegenX PrepX RNA-Seq Library Kit (IntegenX, Pleasanton, Calif.) on an Apollo 324 robotic sample preparation system (WaferGen Biosystems, Fremont, Calif.), closely following kit instructions. Agencourt Ampure XP beads were used for magnetic purification steps (Beckman Coulter, Indianapolis, Ind.). Beads were kept at room temperature for 15 min before starting block setup. Beads were added last to the block, after a 30-sec vortex to fully resuspend them.

Following cDNA synthesis, the concentration of samples was assessed by using a Qubit 1.0 fluorometer (Invitrogen/Thermo Fisher Scientific, Grand Island, N.Y.), high-sensitivity dsDNA reagents (Molecular Probes/Thermo Fisher Scientific, Grand Island, N.Y.), and Qubit Assay Tubes (Invitrogen). Samples were diluted to 20 µg/ml and then sheared on a Covaris S220 Focused ultrasonicator (Covaris, Woburn, Mass.) using a 72-sec protocol and targeting 220/320 bp output. TapeStation HS D1K tape (Agilent) was used to examine sheared DNA for optimal size range. BIOO Scientific NEXTflex DNA barcodes (#514102, Austin, Tex.) were diluted to 5 µm and used in the IntegenX PrepX DNA Library ILM prep kit (#P003279, Pleasanton, Calif.). Library prep was performed on the

Apollo 324 using the kit manufacturer's precise instructions. 5-µl aliquots of ~2-µg/ml samples were then subjected to four PCR amplification cycles by using NEB Next Master Mix (#M0541S, NEB, Ipswich, Mass.) and NEXTflex Primer Mix (BIOO Scientific) and the following cycle conditions: denaturation at 98°C for 120 sec; 5 cycles of 98°C for 30 sec, 6°C for 30 sec, and 72°C for 60 sec; and final extension for 5 min at 72°C. The Agilent Apollo 324 was used for cleanup of PCR samples using the built-in PCR cleanup protocol and Agencourt Ampure XP beads. Libraries were analyzed with Qubit 1.0, TapeStation and qPCR to assess library concentration, size and quality. Samples were each diluted to 0.29 nM concentration and then pooled. Two lanes of 2 x 150 bp Illumina HiSeq 2500 Rapid Run RNA-sequencing (Illumina, San Diego, Calif.) yielded a total 232.4 reads that passed filter.

Sequenced reads were trimmed with Trimmomatic [42] and concatenated. Ribosomal rRNA reads were removed by using Bowtie [43] and a custom database of known rRNA sequences for each species. Transcriptomes were assembled *de novo* using Trinity [44,45]. BLAST databases were created from the *de novo* assemblies and used to identify SFTPC and SFTPC-like sequences.

SFTPC phylogeny

SFTPC sequences were identified through BLASTX, TBLASTN and TBLASTX searches of sequenced transcriptomes from this study (*Plethodon cinereus* and *Ambystoma mexicanum*) as well as from the transcriptomes listed in Table S2.

Sequence identifiers and corresponding sequence data are provided as Supplemental Data File 1.

358 SFTPC sequences from annotated genomes were also taken from NCBI and
359 ENSEMBL (Supplemental Data File 1). Outgroup proteins were selected based
360 on previous phylogenies of SFTPC [46,47]. Predicted amino acid sequences
361 were generated from all nucleotide sequences. Multiple sequence alignment was
362 performed using PRANK [48]; resulting alignments were visually inspected
363 (Supplemental Data File 2). ProtTest was used to identify an appropriate amino
364 acid substitution model [49]. The optimal amino acid substitution model was
365 JTT+G [50], as judged by AIC. Subsequently, 95% maximum clade credibility
366 gene trees were reconstructed in MrBayes (v3.2.6) [51] using Markov chain
367 Monte Carlo analysis with one million generations sampled every 100
368 generations and a relative burn-in of 25%. Convergence of the posterior
369 probabilities was assessed by examining output statistics, including the potential
370 scale reduction factor, which equaled or exceeded 1.000.

371 A phylogeny was also constructed in RAxML (v8.2.9) [52] by using 1000
372 bootstrap replicates and the aforementioned amino acid substitution model. Tree
373 topology was concordant with the Bayesian tree generated in Mr. Bayes.

374 JalView was used to generate the multiple sequence alignment image [53].

375 PHYLDOG [54] was used to estimate gene duplication of SFTPC. A guide tree
376 was constructed using NCBI taxonomy for major groups and [55] for amphibian
377 relationships (Fig. S2). Topology optimization was not used.

378 ***In situ* hybridization**

379 Embryos were fixed overnight in 4% paraformaldehyde (PFA) or MEMFA at 4°C,
380 dehydrated and stored in 70% or 100% MeOH at -20°C. Wholemount mRNA *in*
381 *situ* hybridization (ISH) was performed by rehydrating samples, which were then
382 treated with 5–10 µg/ml proteinase K for 30–60 min, washed with PBTw (137 mM
383 NaCl, 2.7 mM KCl, 10 mM Na_2HPO_4, 1.8 mM KH_2PO_4 and 0.2% Tween-20),
384 post-fixed in 4% PFA, washed with PBTw, and pre-hybridized in hybridization
385 buffer for 2 hr at 65°C (hybridization buffer: 50% formamide, 5x SSC, 0.1 mg/ml
386 heparin, 1x Denhardt solution, 0.01% CHAPS, 0.2 mg/ml tRNA and 0.1% Tween-
387 20; all solutions were RNase-free). DIG-labeled riboprobes were diluted
388 approximately 1:40 in hybridization buffer, denatured at 85°C for 10 min, and
389 then added to specimens. Hybridization was carried out overnight at 65°C.
390 Posthybridization washes were performed with a solution of 50% formamide, 5x
391 SSC and 0.2% Tween-20 at 65°C for eight changes of 30 min each. Specimens
392 were washed with maleic acid buffer plus 0.2% Tween-20 (MABT) prior to
393 blocking and antibody incubation. Antibody block solution included 20% heat-
394 inactivated sheep serum and 2% blocking reagent (Roche, Penzberg, Germany)
395 in MABT. Samples were incubated overnight at 4°C with 1:2500 anti-DIG-AP Fab
396 fragments (Roche) diluted in blocking solution. Extensive washes with MABT
397 were performed prior to color development using BM-Purple (Roche) or
398 NBT/BCIP (Sigma, St. Louis, Mo.). Color development occurred over several
399 hours. Embryos were then embedded for cryosectioning at 14–16 µm thickness.
400 Photographs were taken using a Leica DMRE microscope (Wetzlar, Germany)
401 equipped with a QImaging Retiga 2000r camera and a QImaging RGB slider

(Model: RGB-HM-S-IR; Surrey, Canada) and Volocity 6.0 software (PerkinElmer, Waltham, Mass.).

Structure models

An experimentally determined protein data bank (PDB) model for porcine SFTPC [16] was downloaded from the Research Collaboratory for Structural Bioinformatics PDB. The secondary and supersecondary structure of *Desmognathus fuscus* SFTPC-like was predicted using Quark *Ab initio* Protein Structure Prediction [56]. The N- and C-terminal extent of the *Desmognathus* SFTPC-like sequence was chosen based on alignment with mature forms of SFTPC found in mammals. Protein structure prediction was also performed with I-TASSER [57].

A structure model for *D. fuscus* SFTPC-like was also predicted in SWISS-MODEL [58] using the molecular structure derived by Johansson et al. [16] as a template. The PDB files for each SFTPC-like model were imported into PyMol (Schrödinger) and aligned with the SFTPC model to graphically illustrate structural similarities.

Transmission electron microscopy

Two 24-mm (total length) *Desmognathus fuscus* larvae were euthanized and decapitated. Specimens were then dissected in fixative (2.5% glutaraldehyde and 2% paraformaldehyde in 0.1 M HEPES; the aldehydes were free of alcohol stabilizers). The head was cut into three 1-mm sagittal sections. An 18-cm adult *Ambystoma mexicanum* was euthanized and then dissected in fixative. Samples

of the gular skin from the ventral head, the oral epithelium and the lungs were trimmed to 1-mm-thick pieces in fixative and fixed as above.

The samples were left in fixative for 3 d and then washed twice quickly with 0.1 M HEPES and three times for 5 min each with Milli-Q H_2O (mqH_2O). Next, samples were fixed for 24 hr at 4°C in aqueous 1% osmium tetroxide, followed by five washes in mqH_2O for 5 min each. Subsequently, specimens were stained with 2% uranyl acetate (EMS, Hatfield, Pa.) overnight at 4°C, then washed two times for 5 min each with mqH_2O. Specimens were dehydrated with 5-min washes of 50%, 70% and 95% ethanol, followed by three 10-min washes with 100% ethanol, then two quick rinses with propylene oxide (PO). Specimens were embedded in Embed 812 resin (EMS) formulated to medium hardness by rinsing 30 min each in 1:1 PO to Embed 812, 1:2 PO to Embed 812, then 60 min in 1:4 PO to Embed 812. Specimens were then transferred to 100% Embed 812 and incubated overnight at room temperature, followed by two subsequent changes of Embed 812, over a total embedding time of 48 hr. Samples were then positioned in molds and placed at 60°C for 3 d to polymerize.

Sectioning was performed on a Leica UCT ultramicrotome, using glass knives for trimming blocks and generating semi-thin (1 µm) sections, and a DiATOME diamond knife for generating thin sections of approximately 60–100 nm thickness (target thickness: 80 nm). Sections were flattened with chloroform vapor, transferred onto precoated Formvar/carbon 200 mesh copper grids (#01803F, Ted Pella, Redding, Calif.), and dried on filter paper.

446 Grids were imaged with an FEI Tecnai G2 series F20 transmission electron
447 microscope (Hillsboro, Ore.) at 80 kV using a Gatan CCD camera and Gatan
448 Digital Micrograph Software (Pleasanton, Calif.).

449 **Data Availability**

450 All data are available as Supplemental Data Files 1 and 2.

451

452 **Acknowledgements:** Sequences were provided by Chris Amemiya, John Burns,
453 Paul Hime, Ryan Kerney, Justin Kratovil, Rachel Mueller, Igor Schneider, Randal
454 Voss, David Weisrock, and Ryan Woodcock (Table S2). Carolyn Marks offered
455 help and guidance with TEM. Carolyn Eng assisted with field collection. This
456 work was performed in part at the Harvard University Center for Nanoscale
457 Systems (CNS), a member of the National Nanotechnology Coordinated
458 Infrastructure Network (NNCI), supported under NSF ECCS award no. 1541959.
459 Z.R.L. was supported by the NSF Graduate Research Fellowship Program.

460

461 **Author contributions:** Z.R.L. cloned SFTPC and SFTPC-like from *A.*
462 *mexicanum* and *P. cinereus*, generated and analyzed transcriptomes, performed
463 phylogenetic and structural analyses, performed TEM, collected and raised
464 animals, generated gene expression data and participated in writing the
465 manuscript. J.A.D. cloned SFTPC-like from *D. fuscus* and assisted with
466 characterizing the expression of SFTPC-like. J.H. participated in the data
467 analyses and writing of the manuscript.

468

Competing interests: The authors declare that they have no competing financial interests.

References:

1. Whitford WG, Hutchison VH. 1965 Gas exchange in salamanders. *Physiol. Zool.* **38**, 228–242.
2. Gatz RN, Crawford EC, Piiper J. 1974 Respiratory properties of the blood of a lungless and gill-less salamander, *Desmognathus fuscus*. *Respir. Physiol.* **20**, 33–41.
3. Feder ME, Burggren WW. 1985 Cutaneous gas exchange in vertebrates: design, patterns, control and implications. *Biol. Rev. Camb. Philos. Soc.* **60**, 1–45.
4. Bickford D, Iskandar D, Barlian A. 2008 A lungless frog discovered on Borneo. *Curr. Biol.* **18**, 374–375.
5. Wilder IW, Dunn E. 1920 The correlation of lunglessness in salamanders with a mountain brook habitat. *Copeia* **1920**, 63–68.
6. Reagan NL, Verrell PA. 1991 The evolution of plethodontid salamanders: did terrestrial mating facilitate lunglessness? *Am. Nat.* **138**, 1307–1313.
7. Czopek J. 1965 Quantitative studies on the morphology of respiratory surfaces in amphibians. *Acta Anat. (Basel).* **62**, 296–323.
8. Seelye A. 1906 Circulatory and respiratory systems of *Desmognathus fusca*. *Proc. Bost. Soc. Nat. Hist.* **32**, 335–357.
9. Barrows AI. 1900 Respiration of *Desmognathus*. *Anat. Anz.* **18**, 461–464.

10. Sheafor EA, Wood SC, Tattersall GJ. 2000 The effect of graded hypoxia on the metabolic rate and buccal activity of a lungless salamander (*Desmognathus fuscus*). *J. Exp. Biol.* **203**, 3785–3793.

11. Lombard RE, Wake DB. 1986 Tongue evolution in the lungless salamanders, family Plethodontidae IV. Phylogeny of plethodontid salamanders and the evolution of feeding dynamics. *Syst. Zool.* **35**, 532–551.

12. Wake DB. 1982 Functional and developmental constraints and opportunities in the evolution of feeding systems in urodeles. In *Environmental Adaptation and Evolution* (eds D Mossakowski, G Roth), pp. 51–66. Stuttgart: Gustav Fisher.

13. Daniels CB, Orgeig S, Smits AW. 1995 The evolution of the vertebrate pulmonary surfactant system. *Physiol. Zool.* **68**, 539–566.

14. Whitsett JA, Weaver TE. 2002 Hydrophobic surfactant proteins in lung function and disease. *N. Engl. J. Med.* **347**, 2141–2148.

15. Olmeda B, Villén L, Cruz A, Orellana G, Perez-Gil J. 2010 Pulmonary surfactant layers accelerate O2 diffusion through the air-water interface. *Biochim. Biophys. Acta - Biomembr.* **1798**, 1281–1284.

16. Johansson J, Szyperski T, Curstedt T, Wüthrich K. 1994 The NMR structure of the pulmonary surfactant-associated polypeptide SP-C in an apolar solvent contains a valyl-rich alpha-helix. *Biochemistry* **33**, 6015–6023.

17. Hafner D, Germann PG, Hauschke D, Kilian U. 1999 Effects of early

515 treatment with rSP-C surfactant on oxygenation and histology in rats with
516 acute lung injury. *Pulm. Pharmacol. Ther.* **12**, 193–201.
517 18. Rice WR, Sarin VK, Fox JL, Baatz J, Wert S, Whitsett JA. 1989 Surfactant
518 peptides stimulate uptake of phosphatidylcholine by isolated cells. *Biochim.*
519 *Biophys. Acta* **1006**, 237–245.
520 19. Weaver TE, Whitsett JA. 1991 Function and regulation of expression of
521 pulmonary surfactant-associated proteins. *Biochem. J.* **273**, 249–264.
522 20. Guyton AC, Moffatt DS, Adiar TH. 1984 Role of alveolar surface tension in
523 transepithelial movement of fluid. In *Pulmonary Surfactant* (eds B
524 Robertson, L Van Golde, J Batenburg), pp. 171–185. Amsterdam: Elsevier
525 Science Publishers.
526 21. Ultsch GR, Gros G. 1979 Mucus as a diffusion barrier to oxygen: Possible
527 role in O2 uptake at low pH in carp (*Cyprinus carpio*) gills. *Comp. Biochem.*
528 *Physiol. Part A Physiol.* **62**, 685–689.
529 22. Sosnowski T, Gradon L, Skoczek M, Drozdiel H. 1998 Experimental
530 evaluation of importance of the pulmonary surfactant for oxygen transfer
531 rate in human lungs. *Int. J. Occup. Saf. Ergon.* **4**, 391–409.
532 23. Bourbon JR, Chailley-Heu B. 2001 Surfactant proteins in the digestive
533 tract, mesentery, and other organs: evolutionary significance. *Comp.*
534 *Biochem. Physiol. A, Mol. Integr. Physiol.* **129**, 151–161.
535 24. Fisher JH, Shannon JM, Hofmann T, Mason RJ. 1989 Nucleotide and
536 deduced amino acid sequence of the hydrophobic surfactant protein SP-C
537 from rat: expression in alveolar type II cells and homology with SP-C from

other species. *Biochim. Biophys. Acta* **995**, 225–30.

25. Wert SE, Glasser SW, Korfhagen TR, Whitsett JA. 1993 Transcriptional elements from the human SP-C gene direct expression in the primordial respiratory epithelium of transgenic mice. *Dev. Biol.* **156**, 426–443.

26. Wilder IW. 1925 *The Morphology of Amphibian Metamorphosis*. Northampton: Smith College.

27. Lewis ZR. 2016 Causes and Consequences of Lung Loss in Salamanders. PhD Dissertation. Harvard University.

28. Schmitz G, Müller G. 1991 Structure and function of lamellar bodies, lipid-protein complexes involved in storage and secretion of cellular lipids. *J. Lipid Res.* **32**, 1539–1570.

29. Matoltsy AG, Bednarz JA. 1975 Lamellar bodies of the turtle epidermis. *J. Ultrastructure Res.* **53**, 128–132.

30. Grayson S, Johnson-Winegar AG, Wintroub BU, Isseroff RR, Epstein EH, Elias PM. 1985 Lamellar body-enriched fractions from neonatal mice: preparative techniques and partial characterization. *J. Invest. Dermatol.* **85**, 289–294.

31. Bryant DM *et al.* 2017 A tissue-mapped axolotl de novo transcriptome enables identification of limb regeneration factors. *Cell Rep.* **18**, 762–776.

32. Daniels CB, Orgeig S, Wilsen J, Nicholas TE. 1994 Pulmonary-type surfactants in the lungs of terrestrial and aquatic amphibians. *Respir. Physiol.* **95**, 249–258.

33. Cass AN, Servetnick MD, McCune AR. 2013 Expression of a lung

561 developmental cassette in the adult and developing zebrafish swimbladder.
562 *Evol. Dev.* **132**, 119–132.
563 34. Conant GC, Wolfe KH. 2008 Turning a hobby into a job: How duplicated
564 genes find new functions. *Nat. Rev. Genet.* **9**, 938–950.
565 35. Lan X, Pritchard JK. 2016 Coregulation of tandem duplicate genes slows
566 evolution of subfunctionalization in mammals. *Science* **352**, 1009–13.
567 36. Nehrt NL, Clark WT, Radivojac P, Hahn MW. 2011 Testing the ortholog
568 conjecture with comparative functional genomic data from mammals. *PLoS*
569 *Comput. Biol.* **7**, e1002073.
570 37. Hunter JP. 1998 Key innovations and the ecology of macroevolution.
571 *Trends Ecol. Evol.* **13**, 31–36.
572 38. Lewis ZR, Hanken J. 2017 Convergent evolutionary reduction of atrial
573 septation in lungless salamanders. *J. Anat.* **230**, 16–29.
574 39. Bordzilovskaya N, Dettlaff T, Duhon S, Malacinski G. 1989 Developmental-
575 stage series of axolotl embryos. In *Developmental Biology of the Axolotl*
576 (eds J Armstrong, G Malacinski), pp. 201–219. Oxford: Oxford University
577 Press.
578 40. Nye HLD, Cameron JA, Chernoff EAG, Stocum DL. 2003 Extending the
579 table of stages of normal development of the axolotl: limb development.
580 *Dev. Dyn.* **226**, 555–60.
581 41. Kerney R. 2011 Embryonic staging table for a direct-developing
582 salamander, *Plethodon cinereus* (Plethodontidae). *Anat. Rec.* **294**, 1796–
583 808.

584 42. Bolger AM, Lohse M, Usadel B. 2014 Trimmomatic: a flexible trimmer for
585 Illumina sequence data. *Bioinformatics* **30**, 2114–2120.
586 43. Langmead B, Trapnell C, Pop M, Salzberg SL. 2009 Ultrafast and memory-
587 efficient alignment of short DNA sequences to the human genome.
588 *Genome Biol.* **10**, R25.
589 44. Grabherr MG *et al.* 2011 Full-length transcriptome assembly from RNA-
590 Seq data without a reference genome. *Nat. Biotechnol.* **29**, 644–652.
591 45. Haas BJ *et al.* 2013 De novo transcript sequence reconstruction from RNA-
592 seq using the Trinity platform for reference generation and analysis. *Nat.*
593 *Protoc.* **8**, 1494–512.
594 46. Hughes AL. 2007 Evolution of the lung surfactant proteins in birds and
595 mammals. *Immunogenetics* **59**, 565–72.
596 47. Hedlund J, Johansson J, Persson B. 2009 BRICHOS - a superfamily of
597 multidomain proteins with diverse functions. *BMC Res. Notes* **2**, 180.
598 48. Löytynoja A, Goldman N. 2010 webPRANK: a phylogeny-aware multiple
599 sequence aligner with interactive alignment browser. *BMC Bioinformatics*
600 **11**, 579.
601 49. Abascal F, Zardoya R, Posada D. 2005 ProtTest: selection of best-fit
602 models of protein evolution. *Bioinformatics* **21**, 2104–2105.
603 50. Jones DT, Taylor WR, Thornton JM. 1992 The rapid generation of mutation
604 data matrices from protein sequences. *Bioinformatics* **8**, 275–282.
605 51. Ronquist F *et al.* 2012 MrBayes 3.2: Efficient Bayesian phylogenetic
606 inference and model choice across a large model space. *Syst. Biol.* **61**,

539–542.

52. Stamatakis A. 2006 RAxML-VI-HPC: maximum likelihood-based phylogenetic analyses with thousands of taxa and mixed models. *Bioinformatics* **22**, 2688–90.

53. Waterhouse AM, Procter JB, Martin DMA, Clamp M, Barton GJ. 2009 Jalview Version 2—a multiple sequence alignment editor and analysis workbench. *Bioinformatics* **25**, 1189–1191.

54. Boussau B, Szollosi GJ, Duret L, Gouy M, Tannier E, Daubin V. 2013 Genome-scale coestimation of species and gene trees. *Genome Res.* **23**, 323–330.

55. Pyron RA, Wiens JJ. 2011 A large-scale phylogeny of Amphibia including over 2,800 species, and a revised classification of extant frogs, salamanders, and caecilians. *Mol. Phylogenet. Evol.* **61**, 543–583.

56. Xu D, Zhang Y. 2012 Ab initio protein structure assembly using continuous structure fragments and optimized knowledge-based force field. *Proteins* **80**, 1715–1735.

57. Yang J, Yan R, Roy A, Xu D, Poisson J, Zhang Y. 2015 The I-TASSER Suite: protein structure and function prediction. *Nat. Methods* **12**, 7–8.

58. Arnold K, Bordoli L, Kopp J, Schwede T. 2006 The SWISS-MODEL workspace: a web-based environment for protein structure homology modelling. *Bioinformatics* **22**, 195–201.

Figures:

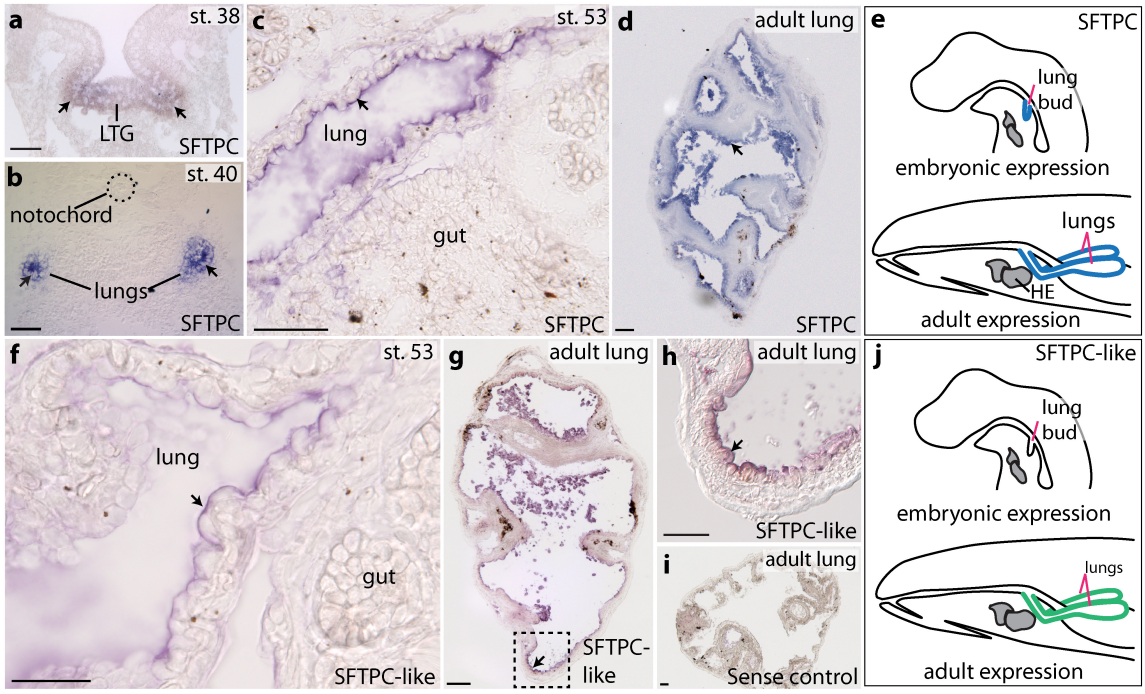

Figure 1. Expression patterns of Surfactant-Associated Protein C (SFTPC) and SFTPC-like in a lunged salamander, *Ambystoma mexicanum*, visualized with antisense wholemount *in-situ* hybridization. Arrows point to representative regions of expression. SFTPC is expressed in the embryonic laryngotracheal groove (LTG) **a,** or lungs **b–d,** of all stages examined between embryo (st. 40), juvenile (st. 53) and adult. **f–h,** SFTPC-like is also expressed specifically in the lung in juveniles and adults, but at a lower level than SFTPC; it is not expressed in embryos. **h,** Boxed region in **g. i,** Negative (sense) control run in parallel with SFTPC-like. **e, j,** Schematic sagittal views summarize the expression sites of SFTPC and SFTPC-like. Blue regions denote high expression; green indicates lower level. **a, b, d** and **g–i** depict transverse sections; **c** and **f** are sagittal sections, anterior to the left. Scale bars: 100 μm. Additional abbreviation: HE, heart.

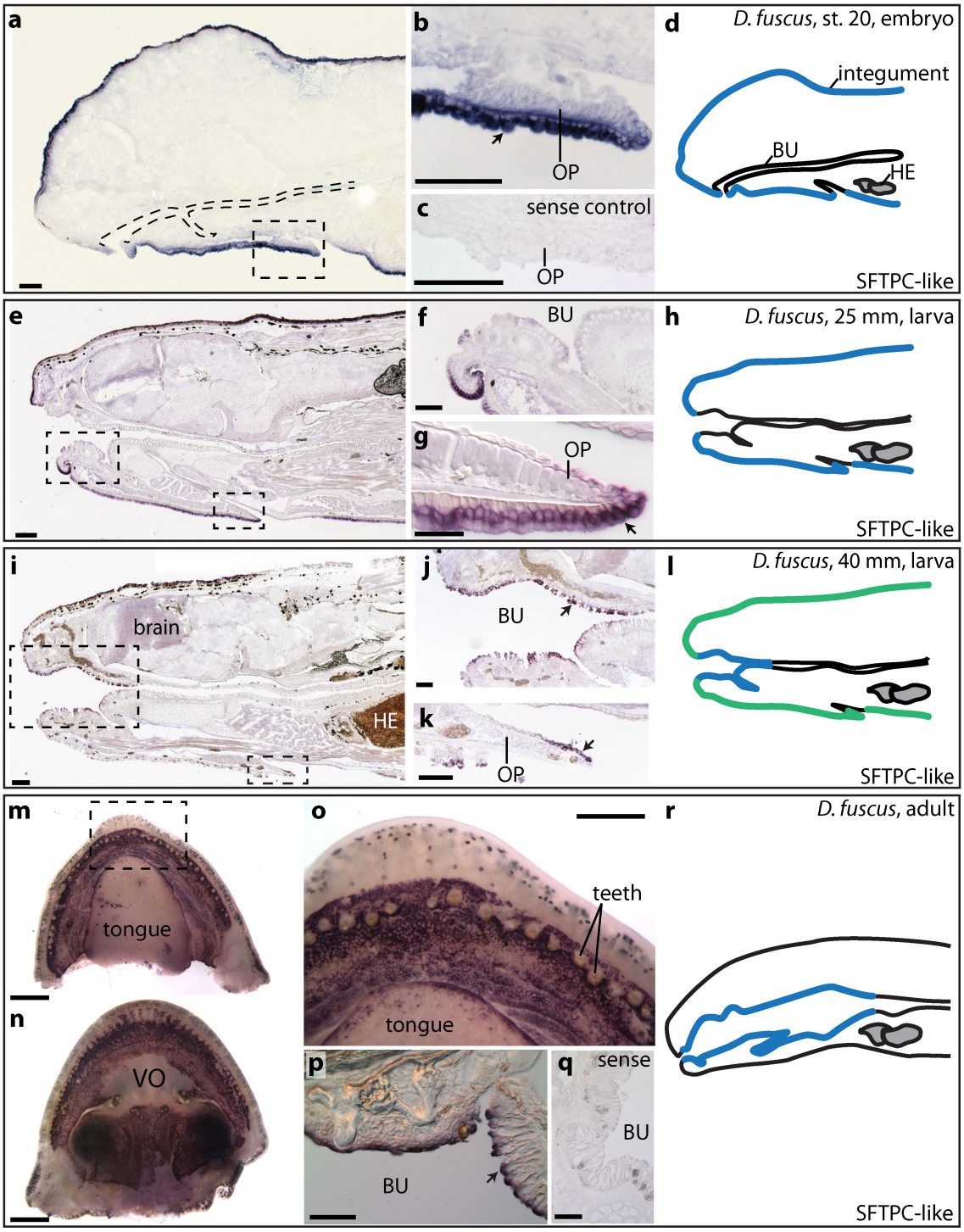

644

645 **Figure 2. Expression of Surfactant-Associated Protein C-like (SFTPC-like)**

646 **in the lungless salamander *Desmognathus fuscus*, visualized with**

647 **antisense wholemount *in-situ* hybridization.** Arrows point to representative

regions of expression. **a–c,** In embryos, SFTPC-like is expressed in the integument. **b,** Boxed region in **a**. **c,** Negative (sense) control. **e–g,** SFTPC-like is expressed in the larval integument, 25 mm total length. **i–k,** SFTPC-like in a larva just prior to metamorphosis, 40 mm total length. Expression has declined in the integument but is now present in the buccopharyngeal mucosa (BU). **m–q,** Adult expression of SFTPC-like is confined to the buccopharyngeal cavity. **d, h, l, r,** Schematic sagittal views summarize the expression sites of SFTPC-like. Blue regions correspond to high expression; green indicates lower level. **a–l** are sagittal sections, anterior to the left; **p** and **q** are transverse sections. Scale bars: **a–c**, **e, f, i–k, p, q,** 100 μm; **g,** 50 μm; **m, n,** 1 mm; **o,** 0.5 mm. Additional abbreviations: HE, heart; OP, opercular covering; VO, vomer.

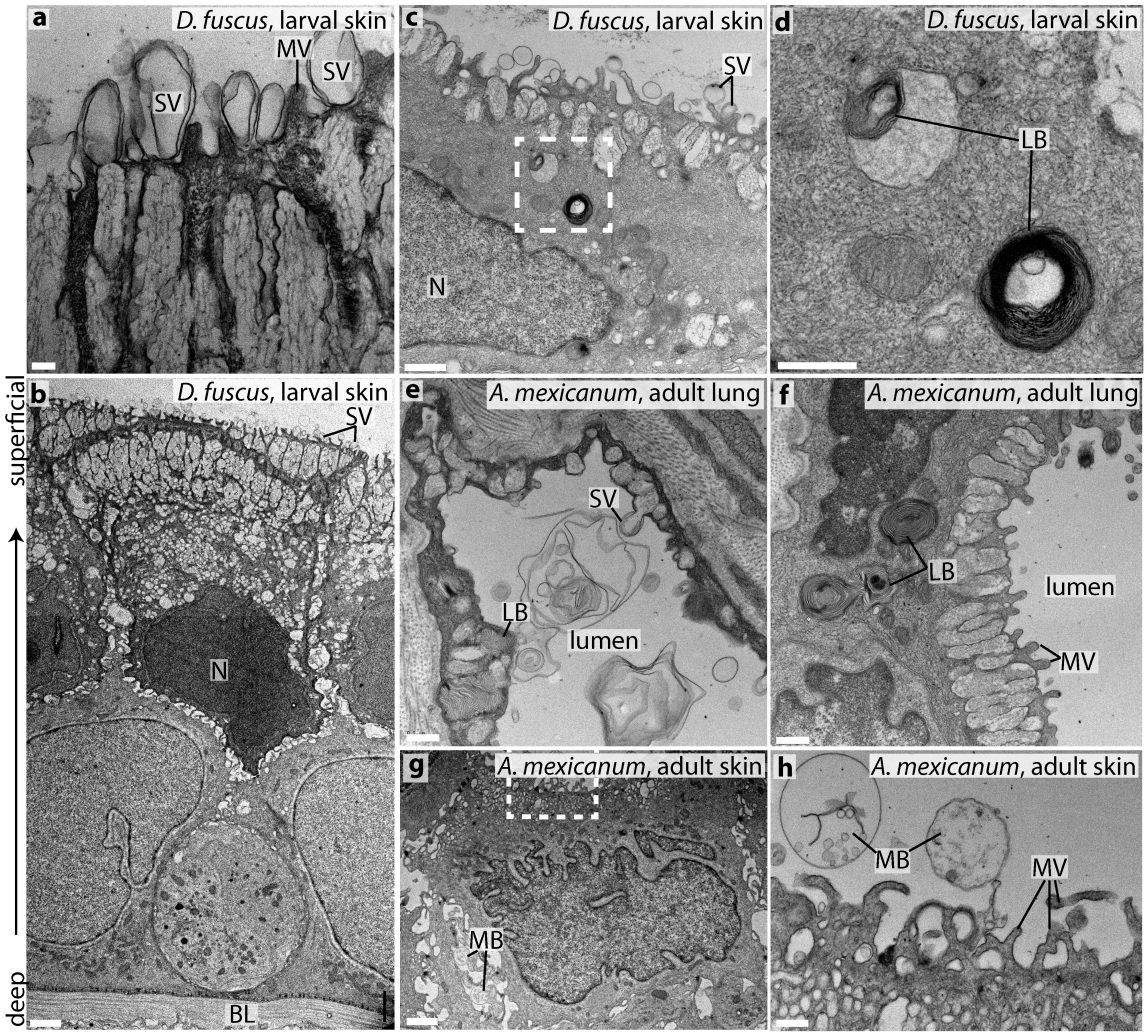

659

660 **Figure 3. Secretory activity and lamellar bodies in the larval integument of**
661 **lungless *Desmognathus fuscus* resemble those in the lung of *Ambystoma***
662 ***mexicanum*. a–d,** Transmission electron micrographs of a 24-mm *D. fuscus*. **a,**
663 The superficial (apical) surface is covered with secretory vesicles (SV), which
664 emerge from columnar vacuolar structures, and is interspersed with microvilli
665 (MV). **b,** Sagittal section through the epidermis; the superficial surface points
666 upwards. **c,d,** Lamellar bodies (LB), indicative of surfactant production, are
667 visible in the integument. The boxed region in **c** is enlarged in **d**. **e,f,** Lamellar
668 bodies and secretory vesicles in the distal portion of the lung of an adult *A.*

669 *mexicanum*; transverse section. **g,h,** Transverse section of gular integument of
670 adult *A. mexicanum*. The boxed region in **g** is enlarged in **h**. Multivesicular
671 bodies (MB) are visible in extracellular spaces in **g** and external to the skin in **h**,
672 but there is no indication of active secretion of vesicles. The integument does not
673 play a pronounced secretory role in this species. Additional abbreviations: BL,
674 basal lamina; N, nucleus. Scale bars: **a,** 200 nm; **b, g,** 2 μm; **c**, 1 μm; **d, e, f, h**,
675 500 nm.

Supporting Information

Supplemental Text

SFTPC expression specificity

The expression pattern of SFTPC is highly conserved: all tetrapods express SFTPC exclusively in the lungs [1–9]. In anamniotes, SFTPC is expressed throughout the lung [5,6,10], whereas in mammals it is confined to alveolar type II cells. Four reports cite expression of SFTPC outside of the lungs in humans, but each report has methodological problems, including possible contamination, that may make such claims unreliable. Mo et al. (2006) report SFTPC in human fetal and adult skin [11]. This claim, however, relies on immunohistochemical data obtained with an antibody that may yield spurious labeling, and on RT-PCR data that was not followed up with sequencing. RT-PCR is subject to contamination and mispriming. Bräuer et al. (2009) report SFTPC expression in submandibular and parotid glands based on RT-PCR and western immunoblots [12]. The western blots reveal a protein of the expected size of the SFTPC pro-protein, and RT-PCR of focal cDNA is performed alongside a positive control, but there is no follow-up sequencing. Schicht et al. (2015) report SFTPC in saliva from human patients based on western blots and ELISA [13]. The antibody used to detect SFTPC is not identified, however, and the isolated band is at 16 kDa while SFTPC proprotein is 21 kDa and mature SFTPC 3.7 kDa [14]. Additionally, saliva may be subject to contamination by surfactant produced in the lungs. Finally, Schob et al. (2013) report SFTPC expression in central nervous system tissue and cerebrospinal fluid based on RT-PCR, but they fail to rule out the possibility of genomic DNA contamination [15]. Their western blots also fail to demonstrate a band at the expected size for SFTPC given the antibody they employed, and the authors express confusion about how mRNA for SFTPC could be present in cerebrospinal fluid. In sum, there are problems with all recent studies that cite extrapulmonary expression of SFTPC in humans. At the same time, numerous studies in mammals and frogs, including ISH and reporter knockins, have failed to demonstrate extrapulmonary expression of SFTPC. For instance, a mouse line with Cre recombinase knocked in to the SFTPC locus fails to label cells outside of the lung when crossed to a reporter line [16]. Nevertheless, it remains possible that humans and perhaps other animals endogenously express SFTPC outside of the lungs. Optimally, *in situ* hybridization and transcriptome sequencing should be used to validate the human results presented above.

Evidence for Duplication of SFTPC

Both SFTPC and SFTPC-like diverge within exonic regions, but not according to putative splice boundaries (Fig. S1a), which indicates that SFTPC-like is not an isoform of SFTPC. While SFTPC-like is divergent from SFTPC sequences, it is not an ortholog of a closely related BRICHOS domain-containing gene (Fig. S1b). We found SFTPC-like expressed in ten species of lunged and lungless salamanders (Fig. S1a, b; Supplemental Data File 1), most of which also express SFTPC. SFTPC-like is not found in genomes or transcriptomes of any other tetrapods, or even other vertebrates.

The most parsimonious explanation for the corresponding gene tree is that the tetrapod ortholog of SFTPC was duplicated in the salamander lineage following its divergence from frogs, followed by substantial sequence divergence between SFTPC and SFTPC-like (Fig. S1b). Low statistical support at the SFTPC-like node should be interpreted as a polytomy, and long-branch attraction likely has caused an artifactual affiliation between coelacanth and lungfish SFTPC orthologs and salamander SFTPC-like. We applied PHYLDOG [17] to explicitly test for gene duplications of SFTPC. Given a guide tree with known phylogenetic relationships (Fig. S2), PHYLDOG predicts that SFTPC-like arose by gene duplication (Fig. S3). SFTPC-like has been meiotically mapped to linkage group 6 in *Ambystoma mexicanum*, a lunged salamander, and is located within a region syntenic to human chromosome 15 [18]. SFTPC-like and SFTPC have been assembled to two separate genomic scaffolds from *A. mexicanum* [19], supporting SFTPC-like's origin via gene duplication.

Supporting Information Tables:

Table S1. Primers used to clone SFTPC and SFTPC-like from *Ambystoma mexicanum, Desmognathus fuscus* and *Plethodon cinereus*.

Gene	Species	Forward	Reverse
SFTPC	*A. mexicanum*	5'-CAC ACA GAR AMG ATT TTC CAG ATG-3'	5'-CGT CTT GTC CAT TTT TGT KAB GTA GCA-3'
SFTPC-like	*A. mexicanum*	5'-AAG ATG GAA ACC GGC AGC AAG C-3'	5'-CGT CTT GTC CAT TTT TGT KAB GTA GCA-3'
SFTPC-like	*D. fuscus*	5'-AAG ATG GAA ACC GGC AGC AAG C-3'	5'-AGT ATT GGA AGC GGT CTG GGT G-3'
SFTPC-like	*P. cinereus*	5'-AAG ATG GAA ACC GGC AGC AAG C-3'	5'-GGT GTA GTC ATA GAC CAC-3'

Table S2. Transcriptomes used to identify SFTPC and SFTPC-like.

Species	Transcriptome Source
Salamanders	
Ambystoma andersoni	Ryan Woodcock and Randal Voss
Ambystoma mexicanum	Present study
Ambystoma tigrinum	Ryan Woodcock and Randal Voss
Ambystoma tigrinum	[20]
Cryptobranchus alleganiensis bishopi	David Weisrock and Paul Hime
Cynops cyanurus	David Weisrock and Paul Hime
Desmognathus fuscus	David Weisrock and Justin Kratovil
Ensatina eschscholtzii	Rachel Mueller [21]
Hynobius chinensis	[22], reassembled by Paul Hime
Hynobius retardatus	[23]
Notophthalmus viridescens	[24]
Plethodon cinereus	Present study
Frogs	
Pelophylax nigromaculatus	[25]
Rana (Lithobates) pipiens	[26]
Dipnoi	
Lepidosiren paradoxa	Igor Schneider [27]
Protopterus annectans	Chris Amemiya [27]

Supporting Information Figures:

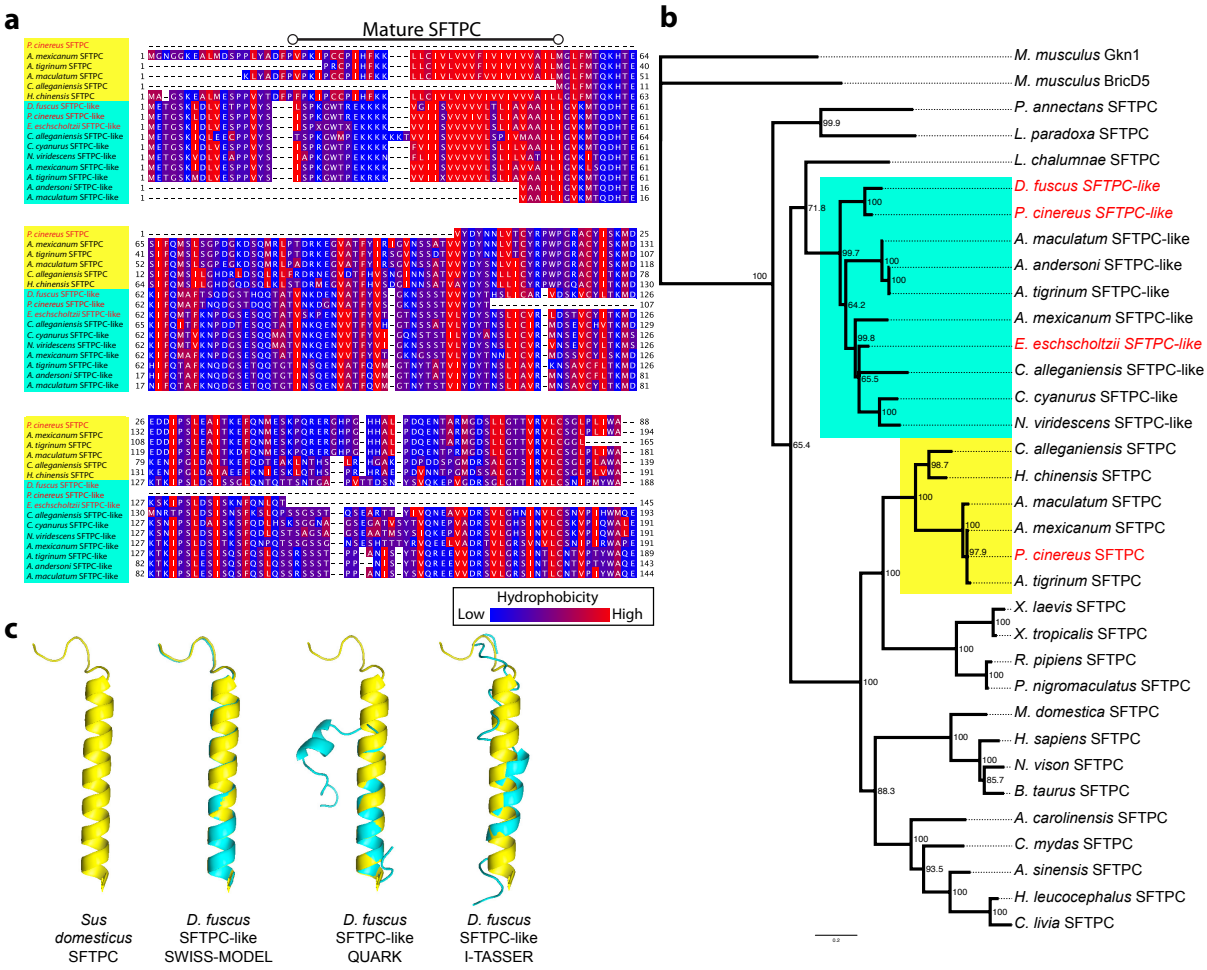

Figure S1. A novel form of Surfactant-Associated Protein C (SFTPC) is expressed in several species of salamanders. a, Amino acid alignment of SFTPC (yellow) and SFTPC-like (cyan) sequences reveals conservation of hydrophobic residues within the mature peptide domain. Full species names and accession numbers are listed in Supplemental Data File 1. Lungless (plethodontid) species are in red font. **b,** Bayesian 95% maximum clade credibility tree for SFTPC reveals SFTPC-like transcripts in 10 species of salamanders. SFTPC-like is not a related ortholog because it is nested within the SFTPC phylogeny. SFTPC-like is not found in any genome or transcriptome outside of salamanders. Node values are posterior probabilities; scale bar is expected changes per site. **c,** Predicted secondary structure of SFTPC-like from *Desmognathus fuscus*. SFTPC-like structure predictions (cyan) utilizing SWISS-MODEL [28], QUARK *Ab initio* predictions [29] and I-TASSER [30] are aligned with the resolved SFTPC mature peptide (yellow) [31].

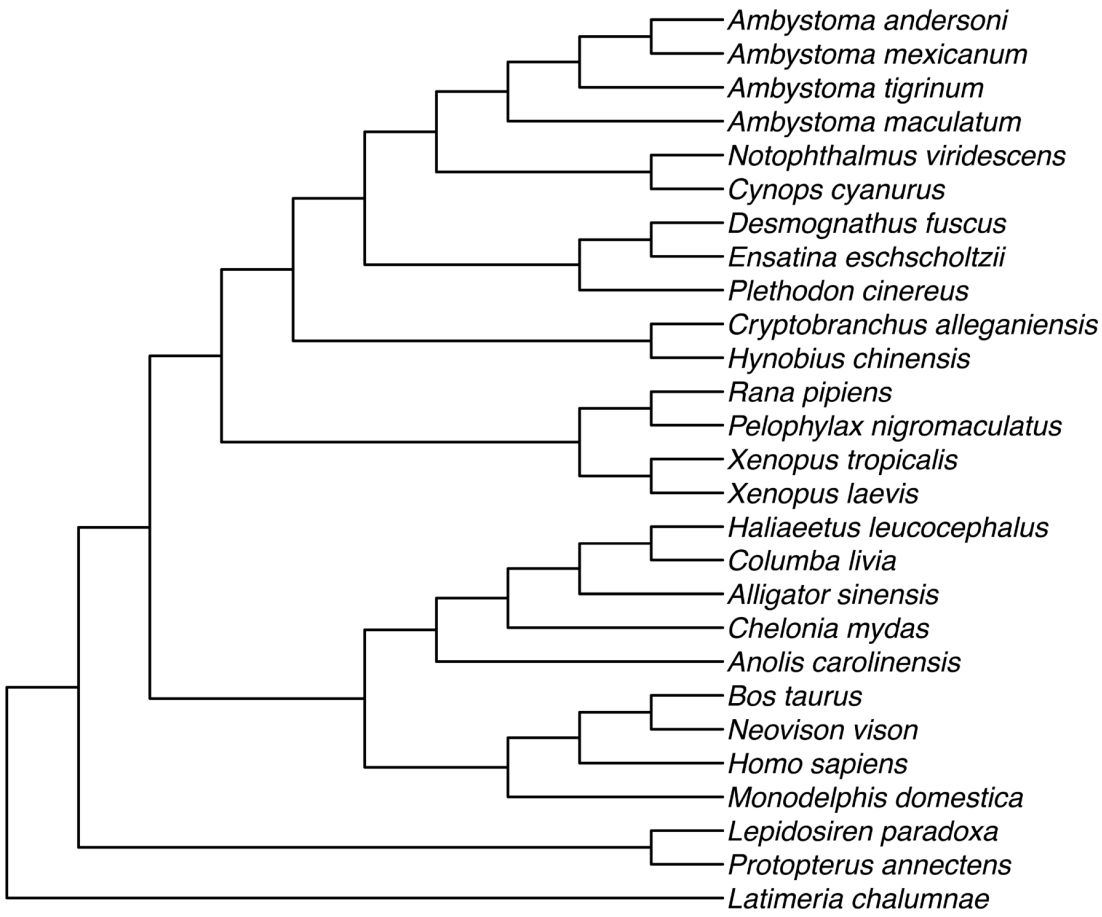

Figure S2. Guide tree for PHYLDOG. NCBI taxonomy was used to generate the tree, combined with Pyron and Wiens (2011) [32] for amphibian taxonomy.

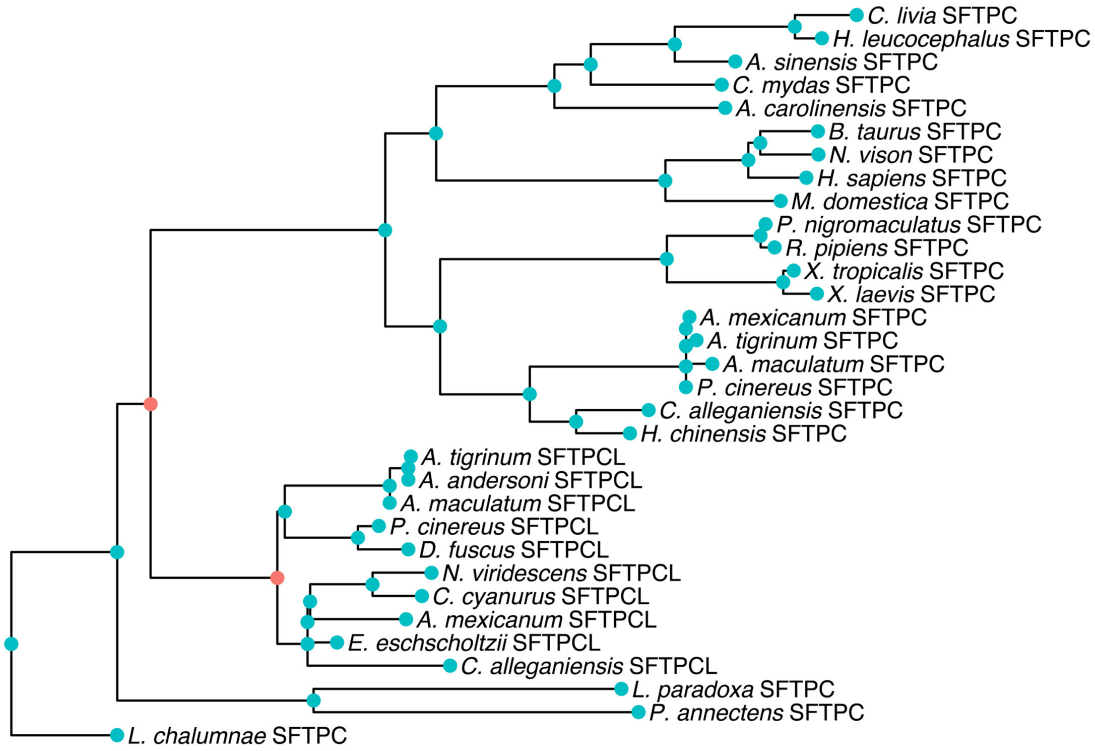

Figure S3. Gene duplications predicted by PHYLDOG. The two nodes where a gene duplication event is predicted are colored red. Blue nodes indicate divergence due to speciation events. PHYLDOG predicts that SFTPC-like (SFTPCL) originated due to gene duplication. A second duplication event of SFTPC-like is predicted in salamanders. While most species of salamanders appear to express only one form of SFTPC-like, several species express SFTPC-like transcripts with slight sequence differences, as noted in Supplemental Data File 1. Further work is needed to determine if these sequence differences can be attributed to further duplications of SFTPC-like or are the result of assembly error or alternative splicing. Only one sequence per species was selected for phylogenetic analysis. Complete species names are provided in Figure S2 and Table S2.

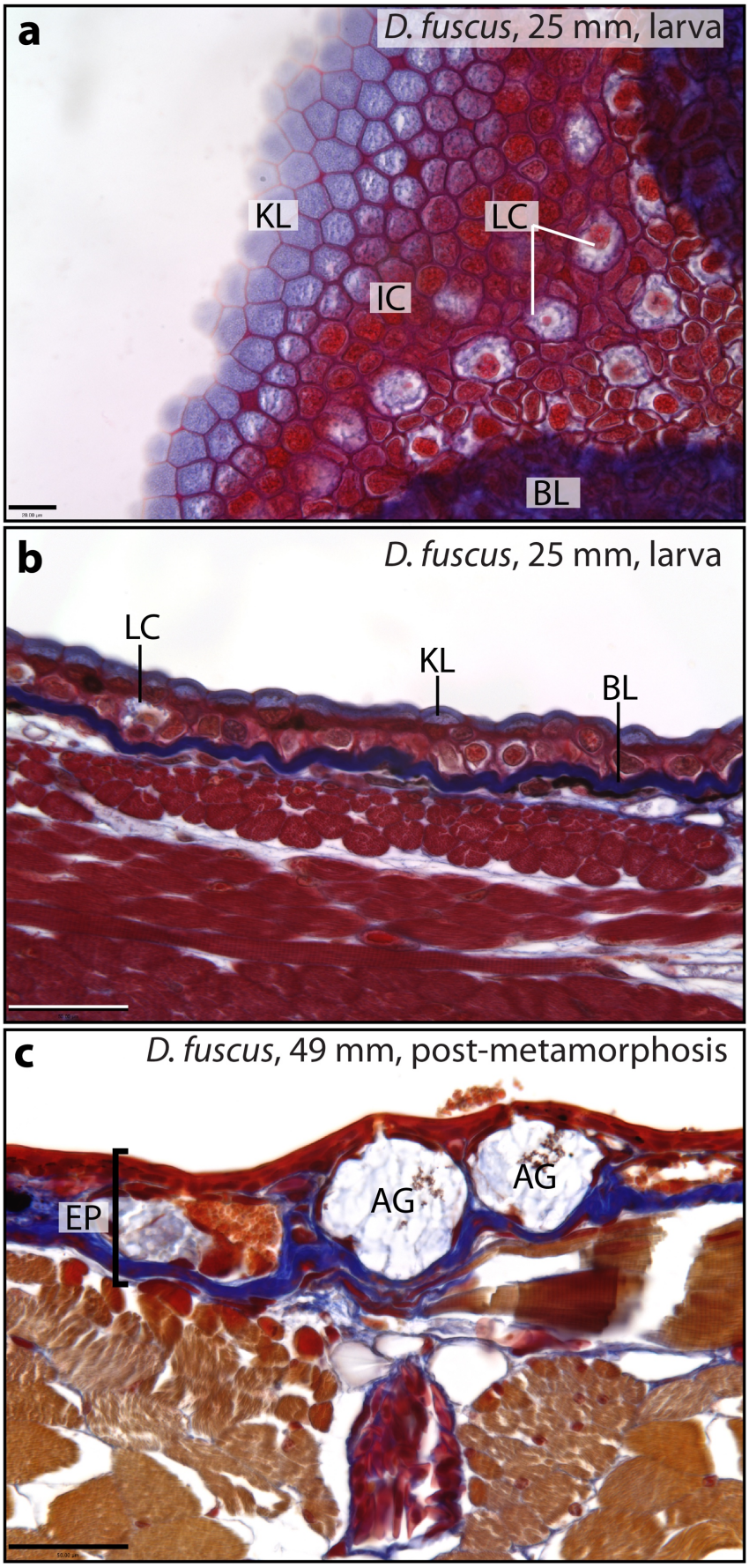

Figure S4. Histology of the integument in *Desmognathus fuscus* before and after metamorphosis. a, Tangential section through the gular region of a larva shows the layers of the integument (from left to right): flattened, cuticle-like keratinized layer (KL); an inner cell layer (IC); large cuboidal Leydig cells (LC) intermingled with capillaries and other supporting cells; basal lamina (BL). **b,** Sagittal section from the abdominal region of a larva. **c,** Transverse section from a recently metamorphosed specimen showing the acinous glands (AG) and a greatly thickened epidermis (EP). Mallory's trichrome stain. Scale bars: **a**, 20 μm; **b,c,** 50 μm.

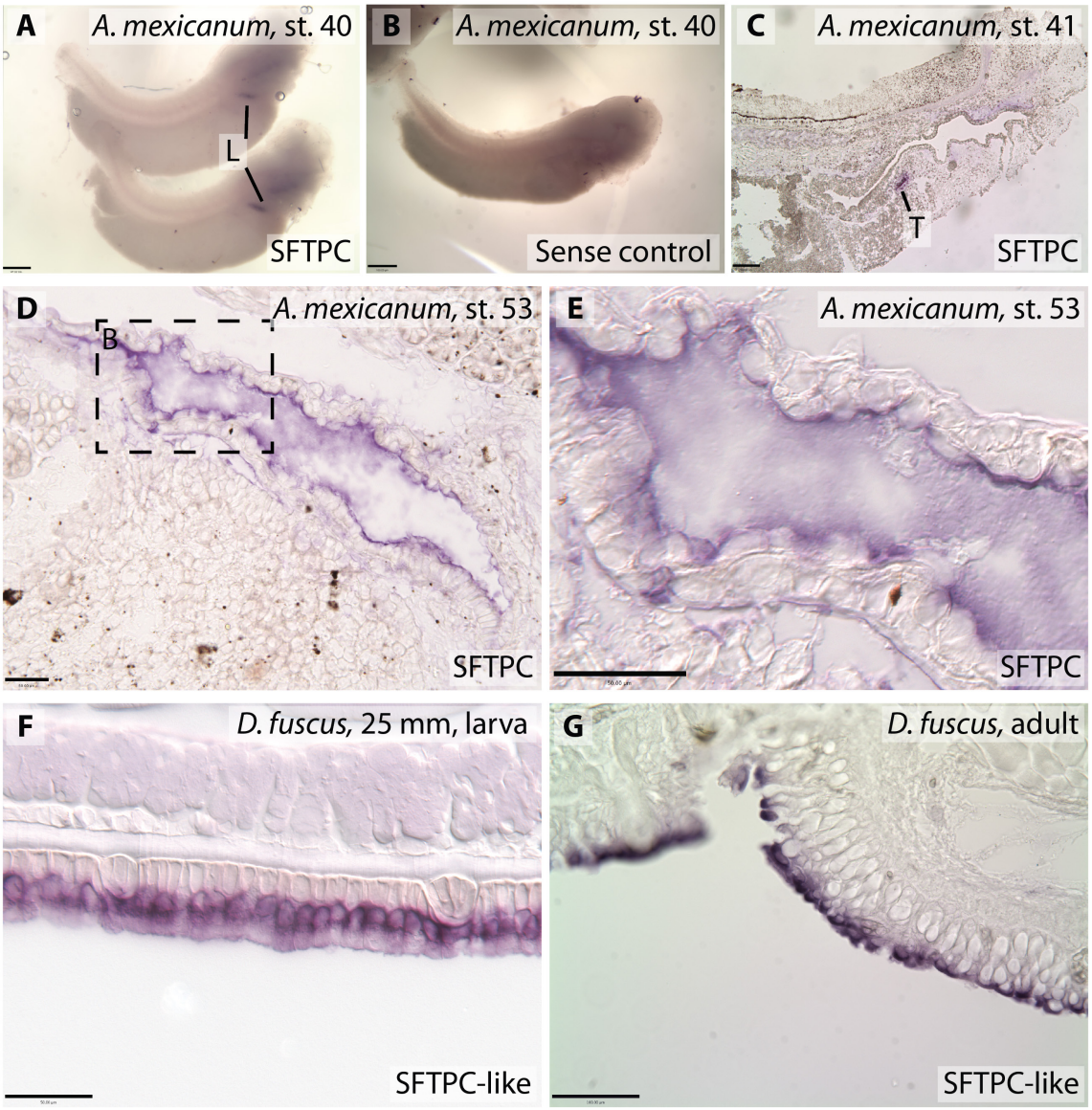

Figure S5. Additional images of SFTPC and SFTPC-like expression patterns. a, Wholemount embryos of *Ambystoma mexicanum* display SFTPC expression specific to the lungs (L). **b**, SFTPC sense control at the same stage shows no lung expression. **c,** Midsagittal section of *A. mexicanum* embryo stained for SFTPC shows expression in the trachea (T), but no expression in the integument or buccopharynx. **d,e,** SFTPC expression in *Ambystoma mexicanum* lung is confined to the squamous epithelial cells lining the lumen. **e** is an enlargement of the boxed region in **d**. **f,** SFTPC-like expression in *Desmognathus fuscus* integument is confined to the apical cellular layer. **g,** SFTPC-like expression in adult *D. fuscus* buccal epithelium. Scale bars: **d,e,f,** 50 μm; **a,b,c,g** 100 μm.

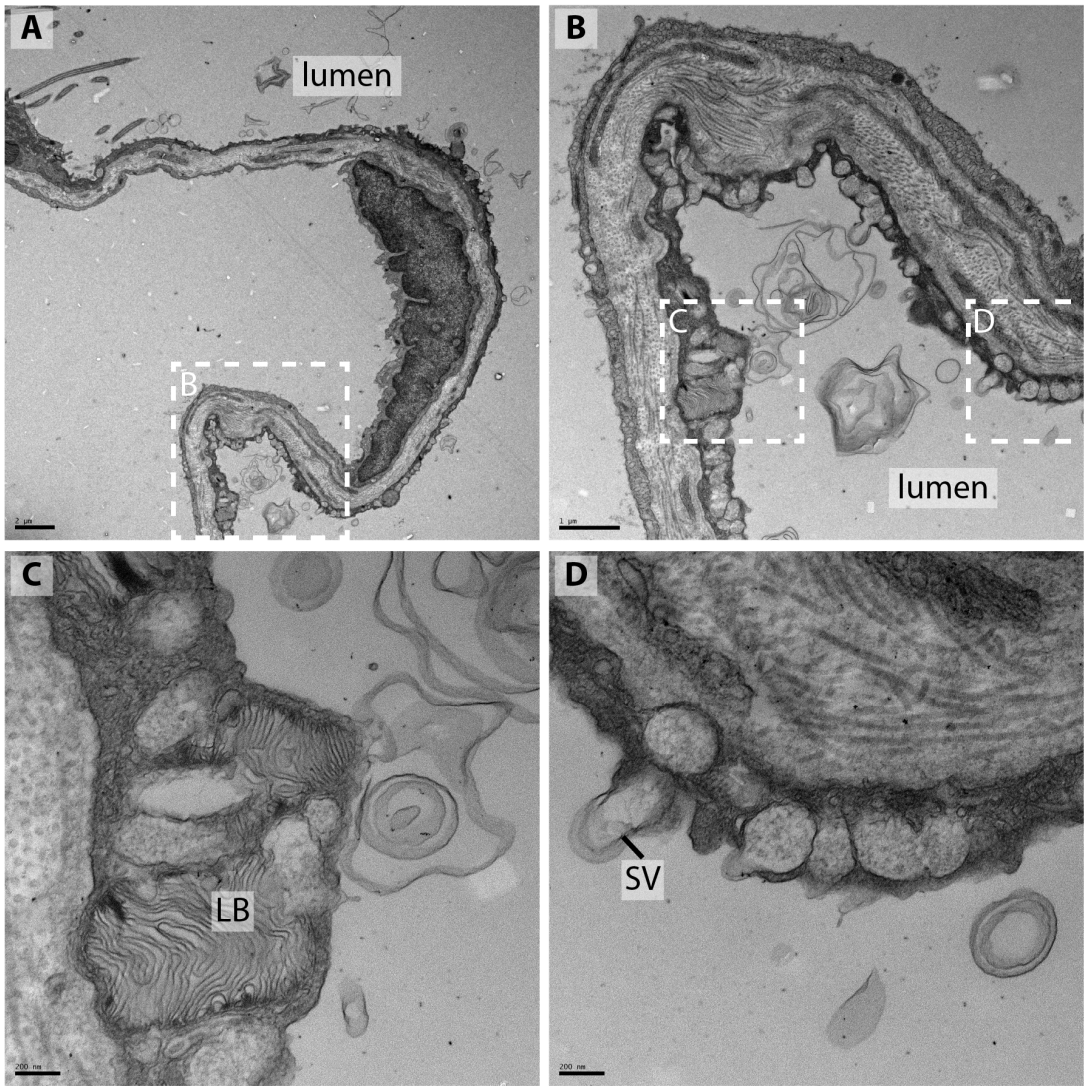

Figure S6. Ultrastructure of alveolar epithelial cells in adult *Ambystoma mexicanum*. **a,** low magnification view of the pulmonary epithelium. The lumen of the lung is to the right. **b,** enlargement of boxed area in **a**. **c,d,** enlargement of boxed regions in **b** show lamellar bodies (LB) and secretory vesicles (SV). Scale bars: **a,** 2 µm; **b,** 1 µm; **c,d,** 200 nm.

Captions for Supplemental Data Files:

Supplemental Data File 1: Excel spreadsheet with all sequence data used for the study.

Supplemental Data File 2: A FASTA amino acid alignment used to generate the gene tree.

Supporting Information References:

1. Bourbon JR, Chailley-Heu B. 2001 Surfactant proteins in the digestive tract, mesentery, and other organs: evolutionary significance. *Comp. Biochem. Physiol. A, Mol. Integr. Physiol.* **129**, 151–161.
2. Fisher JH, Shannon JM, Hofmann T, Mason RJ. 1989 Nucleotide and deduced amino acid sequence of the hydrophobic surfactant protein SP-C from rat: expression in alveolar type II cells and homology with SP-C from other species. *Biochim. Biophys. Acta* **995**, 225–30.
3. Glasser SW, Burhans MS, Eszterhas SK, Bruno MD, Korfhagen TR. 2000 Human SP-C gene sequences that confer lung epithelium-specific expression in transgenic mice. *Am. J. Physiol. Lung Cell. Mol. Physiol.* **278**, L933-45.
4. Wert SE, Glasser SW, Korfhagen TR, Whitsett JA. 1993 Transcriptional elements from the human SP-C gene direct expression in the primordial respiratory epithelium of transgenic mice. *Dev. Biol.* **156**, 426–443.
5. Rankin SA *et al.* 2015 A molecular atlas of *Xenopus* respiratory system development. *Dev. Dyn.* **244**, 69–85.
6. Hyatt BA, Resnik ER, Johnson NS, Lohr JL, Cornfield DN. 2007 Lung specific developmental expression of the *Xenopus laevis* surfactant protein C and B genes. *Gene Expr. Patterns* **7**, 8–14.
7. Weaver TE, Whitsett JA. 1991 Function and regulation of expression of pulmonary surfactant-associated proteins. *Biochem. J.* **273**, 249–264.
8. Wohlford-Lenane CL, Durham PL, Snyder JM. 1992 Localization of Surfactant-associated Protein C (SP-C) mRNA in fetal rabbit lung tissue by in situ hybridization. *Am. J. Respir. Cell Mol. Biol.* **6**, 225–234.
9. Yin A, Winata CL, Korzh S, Korzh V, Gong Z. 2010 Expression of components of Wnt and Hedgehog pathways in different tissue layers during lung development in *Xenopus laevis*. *Gene Expr. Patterns* **10**, 338–44.
10. Rankin SA, Gallas AL, Neto A, Gómez-Skarmeta JL, Zorn AM. 2012 Suppression of Bmp4 signaling by the zinc-finger repressors Osr1 and Osr2 is required for Wnt/β-catenin-mediated lung specification in *Xenopus*. *Development* **139**, 3010–20.
11. Mo YK, Kankavi O, Masci PP, Mellick GD, Whitehouse MW, Boyle GM, Parsons PG, Roberts MS, Cross SE. 2006 Surfactant protein expression in human skin: evidence and implications. *J. Invest. Dermatol.* **127**, 381–386.
12. Bräuer L, Möschter S, Beileke S, Jäger K, Garreis F, Paulsen FP. 2009 Human parotid and submandibular glands express and secrete surfactant proteins A, B, C and D. *Histochem. Cell Biol.* **132**, 331–8.
13. Schicht M *et al.* 2015 The distribution of human surfactant protein within the oral cavity and their role during infectious disease of the gingiva. *Ann. Anat.* **199**, 92–7.
14. Beers MF, Mulugeta S. 2005 Surfactant protein C biosynthesis and its emerging role in conformational lung disease. *Annu. Rev. Physiol.* **67**, 663–696.

15. Schob S, Schicht M, Sel S, Stiller D, Kekulé A, Paulsen F, Maronde E, Bräuer L. 2013 The detection of surfactant proteins A, B, C and D in the human brain and their regulation in cerebral infarction, autoimmune conditions and infections of the CNS. *PLoS One* **8**, e74412.
16. Barkauskas CE, Cronce MJ, Rackley CR, Bowie EJ, Keene DR, Stripp BR, Randell SH, Noble PW, Hogan BLM. 2013 Type 2 alveolar cells are stem cells in adult lung. *J. Clin. Invest.* **123**, 3025–36.
17. Boussau B, Szollosi GJ, Duret L, Gouy M, Tannier E, Daubin V. 2013 Genome-scale coestimation of species and gene trees. *Genome Res.* **23**, 323–330.
18. Voss SR, Kump DK, Putta S, Pauly N, Reynolds A, Henry RJ, Basa S, Walker JA, Smith JJ. 2011 Origin of amphibian and avian chromosomes by fission, fusion, and retention of ancestral chromosomes. *Genome Res.* **21**, 1306–1312.
19. Nowoshilow S *et al.* 2018 The axolotl genome and the evolution of key tissue formation regulators. *Nature* **554**, 50–55.
20. Doyle JM, Siegmund G, Ruhl JD, Eo SH, Hale MC, Marra NJ, Waser PM, Dewoody JA. 2013 Microsatellite analyses across three diverse vertebrate transcriptomes. *Genome* **56**, 407–414.
21. Mohlhenrich ER, Mueller RL. 2016 Genetic drift and mutational hazard in the evolution of salamander genomic gigantism. *Evolution (N. Y).* **70**, 2865–2878.
22. Che R, Sun Y, Wang R, Xu T. 2014 Transcriptomic analysis of endangered Chinese salamander: Identification of immune, sex and reproduction-related genes and genetic markers. *PLoS One* **9**, e87940.
23. Matsunami M, Kitano J, Kishida O, Michimae H, Miura T, Nishimura K. 2015 Transcriptome analysis of predator- and prey-induced phenotypic plasticity in the Hokkaido salamander (*Hynobius retardatus*). *Mol. Ecol.* **24**, 3064–3076.
24. Abdullayev I, Kirkham M, Bjorklund SK, Simon A, Sandberg R. 2013 A reference transcriptome and inferred proteome for the salamander *Notophthalmus viridescens*. *Exp. Cell Res.* **319**, 1187–1197.
25. Huang L, Li J, Anboukaria H, Luo Z, Zhao M, Wu H. 2016 Comparative transcriptome analyses of seven anurans reveal functions and adaptations of amphibian skin. *Sci. Rep.* **6**, 24069.
26. Christenson MK *et al.* 2014 De novo assembly and analysis of the Northern leopard frog *Rana pipiens* transcriptome. *J. Genomics* **2**, 141–9.
27. Amemiya CT *et al.* 2013 The African coelacanth genome provides insights into tetrapod evolution. *Nature* **496**, 311–316.
28. Arnold K, Bordoli L, Kopp J, Schwede T. 2006 The SWISS-MODEL workspace: a web-based environment for protein structure homology modelling. *Bioinformatics* **22**, 195–201.
29. Xu D, Zhang Y. 2012 Ab initio protein structure assembly using continuous structure fragments and optimized knowledge-based force field. *Proteins* **80**, 1715–1735.
30. Yang J, Yan R, Roy A, Xu D, Poisson J, Zhang Y. 2015 The I-TASSER

Suite: protein structure and function prediction. *Nat. Methods* **12**, 7–8.

31. Johansson J, Szyperski T, Curstedt T, Wüthrich K. 1994 The NMR structure of the pulmonary surfactant-associated polypeptide SP-C in an apolar solvent contains a valyl-rich alpha-helix. *Biochemistry* **33**, 6015–6023.

32. Pyron RA, Wiens JJ. 2011 A large-scale phylogeny of Amphibia including over 2,800 species, and a revised classification of extant frogs, salamanders, and caecilians. *Mol. Phylogenet. Evol.* **61**, 543–583.